RSC Advances

ROYAL SOCIETY OF CHEMISTRY

www.rsc.org/advances

Preparation of montmorillonite-pillared graphene oxide with increased single- and co-adsorption towards lead ions and methylene blue

Lu Liu[a], Yaru Zhang[a], Yanjin He[a], Yongfen Xie[a], Langhuan Huang[a], Shaozao Tan[a,*], Xiang Cai[b,*]

[a] Department of Chemistry, Jinan University, Guangzhou 510632, PR China

[b] Department of Light Chemical Engineering, Guangdong Polytechnic, Foshan 528041, P. R.China

Corresponding Author

*E-mail: tanshaozao@163.com (S. Tan) and cecaixiang@163.com (X. Cai)

Abstract

In order to prevent the aggregation of graphene oxide (GO) during storage or application, montmorillonite (MMT) was used as the modifier, and MMT-pillared GO (GM) was prepared. The features of GM were characterized using fourier transform infrared, scanning electron microscope, transmission electron microscopy, energy dispersion X-ray spectrometer, atomic force microscopy and X-ray diffraction measurements. Then, a batch system was applied to study the adsorption behaviors of lead ion (Pb^{2+}) and methylene blue (MB) by GM in single and binary systems. The results showed that GM possessed a higher Brunauer-Emmett-Teller (BET) specific surface area than GO. In the single system, the maximum adsorption capacities of GM for MB and Pb^{2+} were 350 and 285 mg/g, respectively. With the increase of storage day, the BET specific surface area and the maximum adsorption capacity of GM approximately remained unchanged, while the GO was dramatically decreased. For binary system, the presence of MB in water would provide additional binding site for Pb^{2+}, promoting the adsorption of Pb^{2+} on GM. The presence of Pb^{2+} in water would compete with MB on GM during the adsorption process, resulting in a decrease in the adsorption of MB. Adsorption results recorded under different condition indicated that this experiment was capable of simultaneous removal of Pb^{2+} and MB using GM as the adsorbent. In addition, the pillared structure of GM greatly enhanced the noncovalent adhesion.

1. Introduction

Potentially toxic metals represent an important group of pollutants that are commonly found in surface waters contaminated with natural or industrial sources.[1-3] Among various metals, lead is one of the most dangerous pollutants. Even at low concentration, lead is extremely toxic, causing behavioral change, learning disability, development defect, language difficulty, mental retardation and abnormality in pregnant women.[4, 5] Dyes have become one of the main sources of severe water pollution as a result of the rapid development of the textile industry and their low production cost, brighter colour, better resistance towards environmental factor and easy-to-apply factor.[1, 2] Among them, methylene blue (MB) has the widest application, which includes coloring paper, temporary hair colourant, dyeing cotton, wool and coating for paper stock. The presence of dye in water, even at very low concentration, is highly visible and undesirable.[6, 8]

In the past years, several technologies have been employed for removal of potentially toxic metal and dye from aqueous solution, such as adsorption, ion exchange, chemical precipitation and membrane separation.[9-11] Among them, adsorption is usually the simplest and the most cost-effective technique. In addition, adsorption does not result in secondary pollution by producing harmful substance during the process.[12] Numerous works have presented results for the adsorption of dye or potentially toxic metal onto various materials like activated carbon, natural and synthetic polymer, clay mineral or its modified composite, zeolite, agricultural and industrial by-product.[13-18]

Clay minerals (e.g., montmorillonite (MMT)) are good adsorbents for metal ion from aqueous solution owing to the high cation-exchange capacity, high abundance, local availability, nontoxicity, chemical and mechanical stability, low cost and the ability to be recycled.[19, 20] In the past few years, graphene oxide (GO) and graphene nanosheet have attracted tremendous interest in the world. Some reviews on graphene-based material as adsorbent for removal of pollutant are available.[21] The main shortcoming of GO are the agglomeration during storage or application, which will result in the decline of adsorption capacity in practical application. In order to solve the problem, physical[22] or chemical[23, 24] modification of GO was used, but the results are still not ideal. Therefore, it is necessary to probe new method which can solve above problem. What's more, most of these studies only deal with single-component aqueous solution, so, the development of

bi-functionalized adsorbent that is capable of enabling simultaneous removal of two kinds of environmental pollutant has become an emerging frontier in the field of water treatment, and limited works have been published about dealing with the adsorption of dye[25-29] or toxic metal [30, 31] in multi-component aqueous system. For more specific and complicated studies, few literatures have been investigated about the utilization of GO and MMT composite for removal of potentially toxic metal and dye.

In this study, MMT was used as the modifier, and MMT-pillared GO (GM) was prepared. Then, we used GM as adsorbent to simultaneously remove the potentially toxic metal ion and dye. The MB and lead ion (Pb^{2+}) were chosen as typical dye and potentially toxic metal ion, and their adsorption in single and binary systems were compared to investigate simultaneous adsorption process. As a new type of material, the GM combined the properties of the MMT and GO, owned higher adsorption efficiency than GO and MMT after long-term storage, and possessed high adsorption efficiency for the Pb^{2+} and MB than GO and MMT.

2.0 Experiment section

2.1. Materials

The MMT with a cation-exchange capacity (CEC) of 100 meq/100 g on dry basis (dried at 110 °C) was obtained from Hongyu Clay Co., Ltd. (Zhejiang, China). Graphite powder (spectral pure), $KMnO_4$, P_2O_5, concentrated H_2SO_4, H_2O_2, MB and lead nitrate (Pb^{2+}) were purchased from Sinopharm Chemical Reagent Co., Ltd. (Shanghai, China). All MB and Pb^{2+} aqueous solutions used in this study were prepared by dissolving a certain amounts of MB and Pb^{2+} in deionized water. All the reagents were used without further purification. The deionized water used for the preparation of reagent was purified by Millipore reverse osmosis (RO).

2.2. Preparation of GM

GO was synthesized from natural graphite powder by a modified Hummers method.[32-35] In brief, 115 mL of concentrated H_2SO_4 was added into a 500 mL flask containing 5 g of graphite powder and 5 g of P_2O_5, and the mixture was stirred in an ice bath. Then, 25 g of $KMnO_4$ was added slowly into the above mixture. The rate of addition was carefully controlled to keep the reaction temperature below 3 °C.

Afterwards, the temperature was raised to 35 °C and the solution was kept stirring for 2 h at 35 °C. Next, the temperature was continued to rise to 80 °C. When the mixture became reddish brown suspension, 200 mL of H_2O and 5 mL of 30 % H_2O_2 were added to the mixture. And the mixture was washed and centrifuged with deionized water for several times. After filtrated and dried under vacuum, GO was obtained as a solid. Finally, 0.05 g GO was mixed with 1 g MMT in a flask and dispersed in 80 mL of H_2O. After sonicated for 8 h, the mixture was vacuum dried at 60 °C for reserve, the resulting product was named as GM.

2.3. Characterization

Fourier transform infrared (FTIR) spectra were measured with a Bruker Vertex 70 FT-IR spectrophotometer using the KBr method. The morphologies of the samples were observed by scanning electron microscope (SEM) using PHILIPS XL-30 scanning electron microscopy and transmission electron microscopy (TEM) using TECNAI-10 transmissing electron microscopy. Energy dispersive X-ray (EDX) spectra were measured with a Oxford ISIS-300 Energy dispersive X-ray spectrometer. X-ray diffraction (XRD) patterns were obtained on a PANalytical'sX'Pert Power X-ray Diffraction (40 kV, 30 mA) with Cu K_α radiation at a scanning rate of 2.4 °/min. A continuous scan mode was applied to collect 2θ data from 2° to 40°. Atomic Force Microscopy (AFM) images were observed by an atomic force microscope (Benyuan CSPM5500) on a flat mica substrate. Brunauer-Emmett-Teller (BET) specific surface area was determined using Micromeritics ASAP 2010 instrument. Zeta potential measurements were performed using a zeta sizer nano ZS (Malvern Instruments), and all the aqueous samples were diluted to 0.05 mg/mL before measurements.

2.4. Adsorption experiment

The adsorption tests of dye and potentially toxic metal onto the GM were conducted in batch experiment at 30 °C. In single system, a series of 100 mL solution in 250 mL flask were used and each flask was filled with GM at various mass loadings and dye or Pb^{2+} solution at different initial concentration. The conical flasks were agitated in an orbital shaker at 150 rpm and reacted at a given time interval. The suspension was centrifuged at 4500 g for 10 min to separate liquid from solid phase, and then the supernatant liquid was analyzed for MB and Pb^{2+}. MB was determined

spectrophotometrically by measuring the absorbance at λ_{max} = 664 nm (Spectronic 20 Genesys Spectrohotometer), while Pb^{2+} was measured using atomic absorption spectrometry at λ_{max} = 217 nm (SpectrAA110, Varian).

In co-adsorption experiment, GM with various mass loadings was added into a test solution (100 mL) containing Pb^{2+} and MB. The procedures for adsorption and analysis were kept the same as described above.

At equilibrium, the adsorbed amount of dye or potentially toxic metal per unit mass of adsorbent (q_e, mg/g) was determined according to the following mass balance:

$$q_e = \frac{(C_0 - C_e)V}{M} \quad (1)$$

where V was the liquid volume (L), C_0 was the initial concentration in the solution (mg/L), C_e was the equilibrium concentration (mg/L), and M was the amount of the adsorbent sample on a dry basis (g), respectively.

3.0 Results and discussion

3.1. Characterization of GM

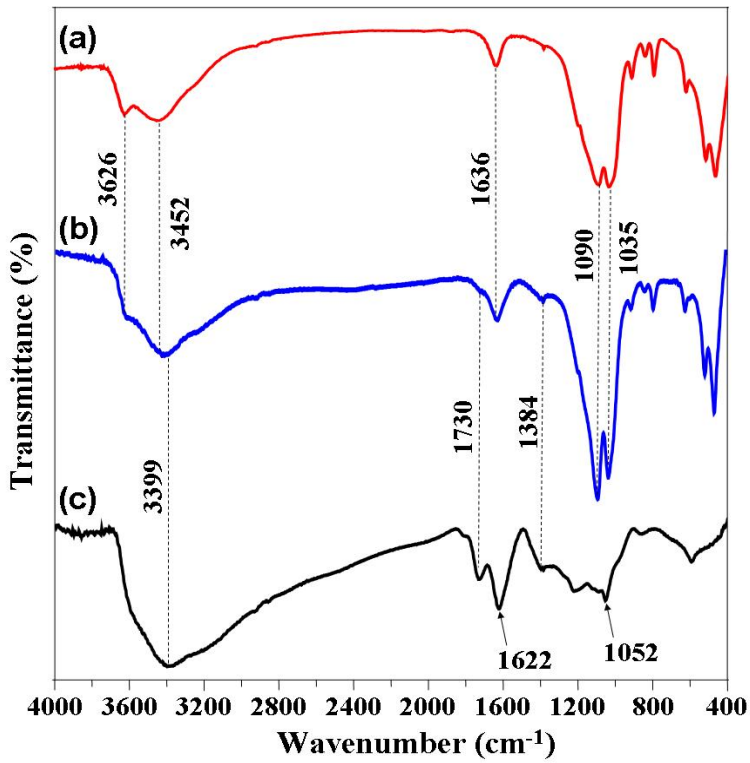

Fig. 1. The FTIR spectra of the MMT (a), GM (b) and GO (c).

The FTIR spectroscopy was carried out for confirming the composition of the GM. According to the FTIR spectrum of MMT (Fig. 1a), the characteristic vibration bands of the MMT were appeared at 3626 cm^{-1} (-OH stretch of the lattice hydroxyl), 3452 cm^{-1} (-OH stretch from free H_2O), 1636 cm^{-1} (-OH bending) and 1035 cm^{-1} (Si-O stretch). In the FTIR spectrum of GO (Fig. 1c), a broad and intensive peak appeared at 3399 cm^{-1} was assigned to -OH stretching band, which might originate from water molecules adsorbed inside GO. Besides, peaks at 1730, 1622, 1384 and 1052 cm^{-1} were corresponded to C=O, C-OH, C=C and C-O-C vibration frequency, respectively. These peaks suggested that graphite had been already oxidized to GO.[32-36] In the FTIR spectrum of GM (Fig. 1b), all the peaks of GO and MMT were appeared, and the bands of peaks belonging to GO became weak. These results illustrated that GO had been composited with MMT.

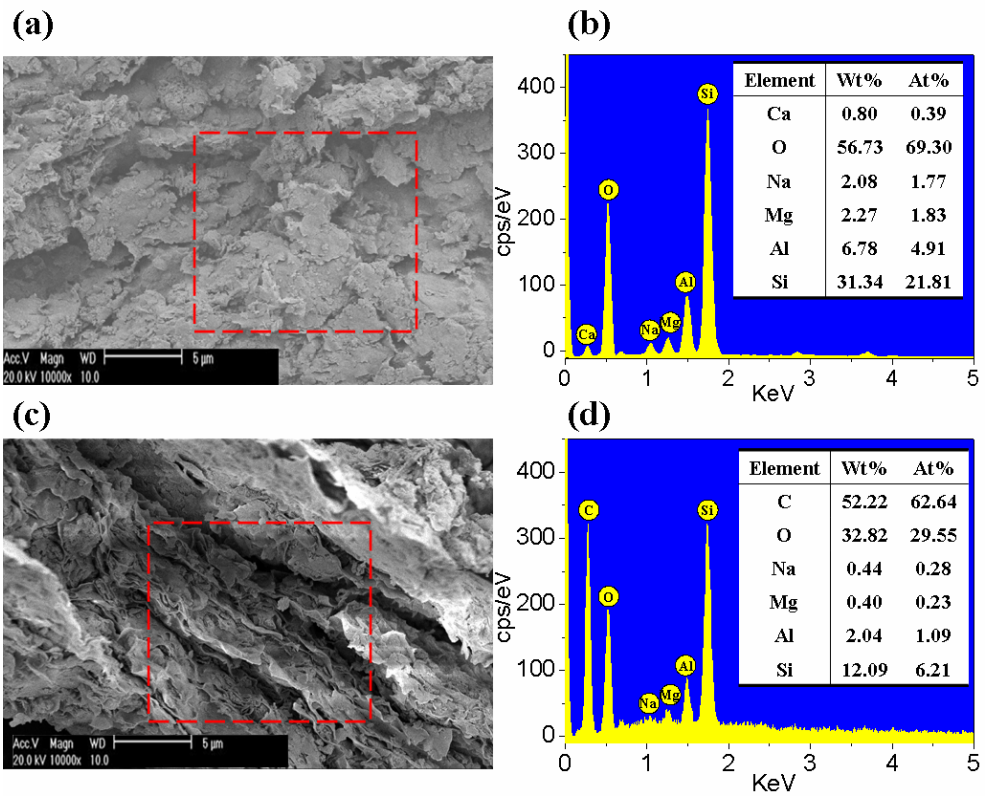

Fig. 2. SEM micrographs of MMT (a) and GM (c). EDX spectra of MMT (b) and GM (d).

The representative SEM image of MMT was shown in Fig. 2a. Fig. 2b showed the EDX spectrum of MMT, revealing MMT contained elements of Ca, O, Na, Mg, Al and Si, which meant it was a calcium montmorillonite.[37] The representative SEM image of GM was shown in Fig. 2c for a high magnification. The GM contented a mass of wrinkles on the surface and in the interlayer sheets, which suggested to be GO. The layered structure of the GM exhibited a much rougher surface, which would provide more active sites for the adsorption of dye or potentially toxic metal ion and help to enhance the adsorption activity of GM. Fig. 2d showed the EDX spectrum of GM, revealing GM contained elements of C, O, Mg, Al and Si. The presences of Si, Mg and Al atoms corroborated the existence of MMT, and the element of C could be related to GO.

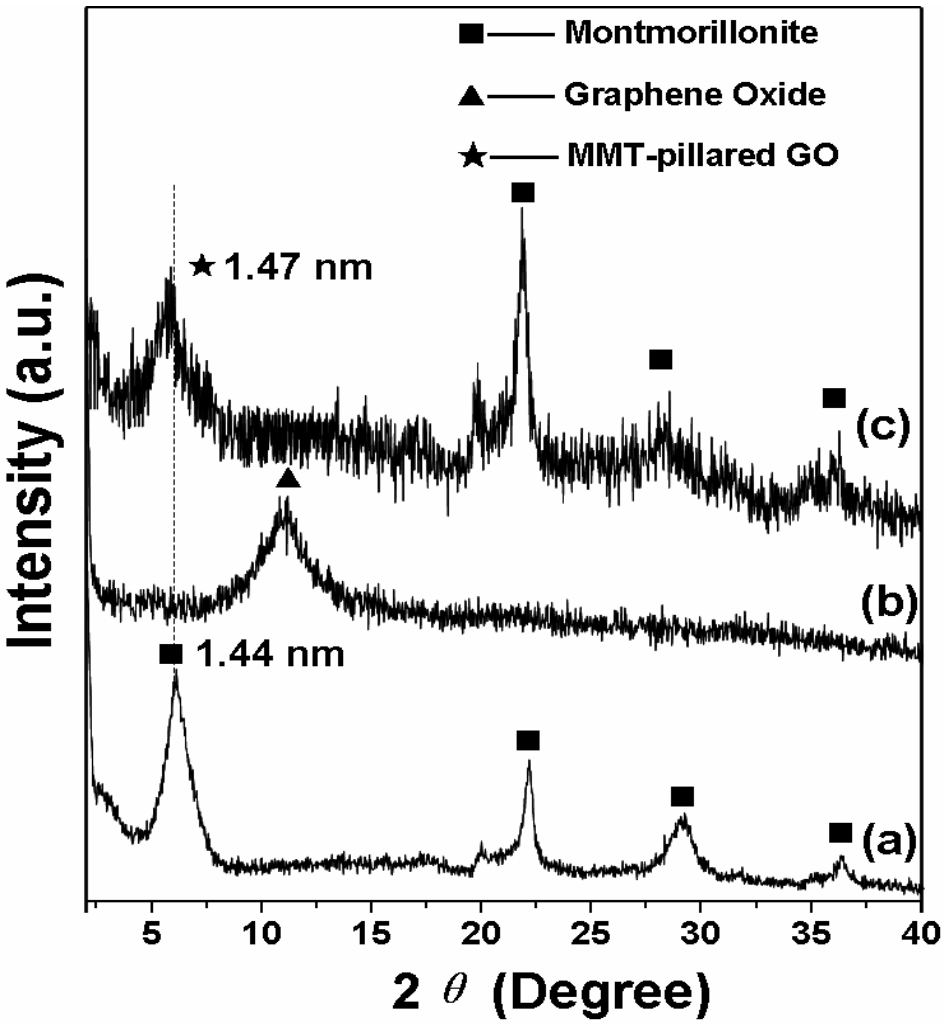

Fig. 3. XRD patterns of the MMT (a), GO (b) and GM (c), which were all sonicated for 8 h.

The XRD patterns of the MMT, GO and GM were presented in Fig. 3. For GO, it could be found a diffraction peak at 2θ=11.00°, corresponding to an interplanar spacing of 0.80 nm (Fig. 3b). For MMT, a typical well-defined d_{001} diffraction peak at 6.12° was consistent with a basal spacing of 1.44 nm (Fig. 3a), which manifested this was a calcium montmorillonite.[37] As for GM, the characteristic peak of MMT was still existed but weakened, while the characteristic peak of GO was disappeared (Fig. 3c), and the d_{001} diffraction peak appeared at 6.07° with 1.47 nm basal spacing, which suggested block of MMT was pillared in every layer of the GO, resulting in the MMT-pillared GO.

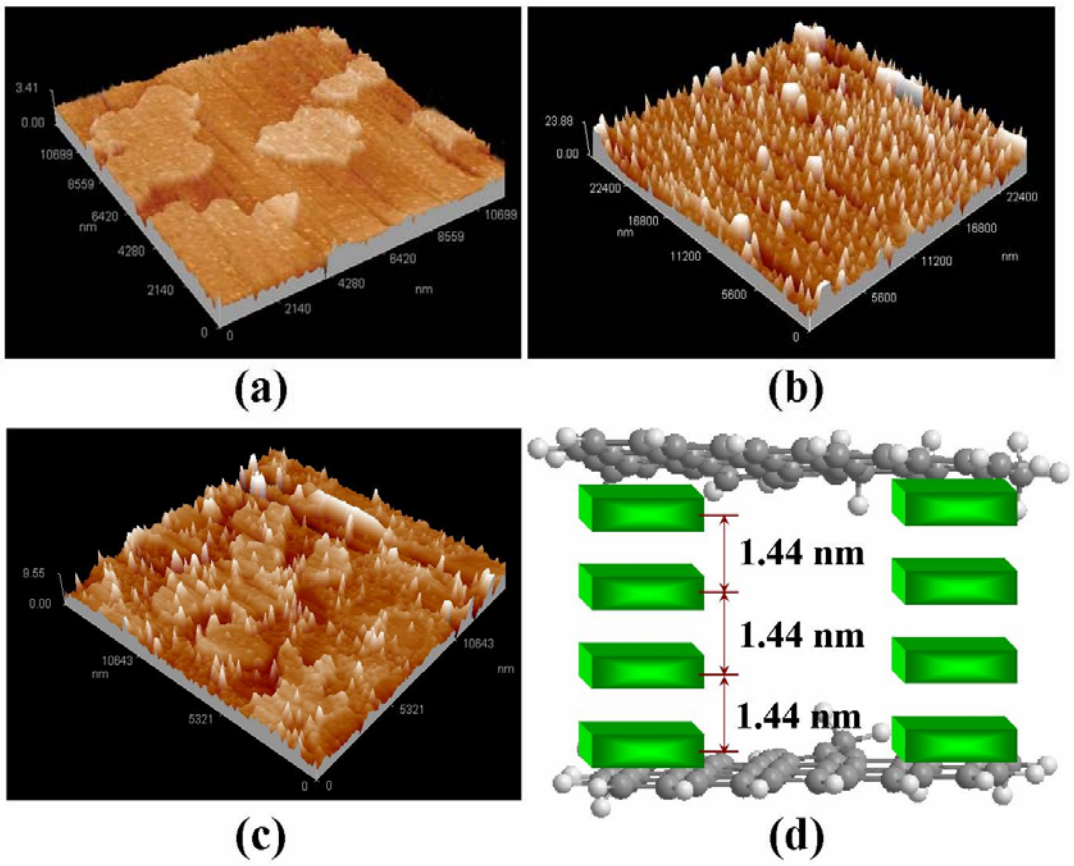

Fig. 4. Tapping-mode AFM image of (a) GO，(b) MMT and (c) GM on a clean mica surface. (d) The schematic of GM.

In order to further illustrate the above XRD results, AFM and TEM were used. As shown in Fig. 4, the representative results of the AFM images for samples prepared from

GO, MMT and GM dispersion in water. The size of GO was about 3~4 μm (length) × 2~3 μm (width) × 1.0~1.2 nm (high); and the size of MMT was about 0.2~0.3 μm (length) × 0.2~0.3 μm (width) × 15~25 nm (high). The image of GO was in flake and MMT was sharp (Fig. 4a and 4b), while the image of GM revealed the presence of GO sheet and the sharp of MMT, and MMT was deeply embedded in each of the GO (Fig. 4c). We suggested that MMT was pillared in every layer of the GO and formed a stable structure (Fig. 4d). This conclusion was consistent with the SEM and XRD results.

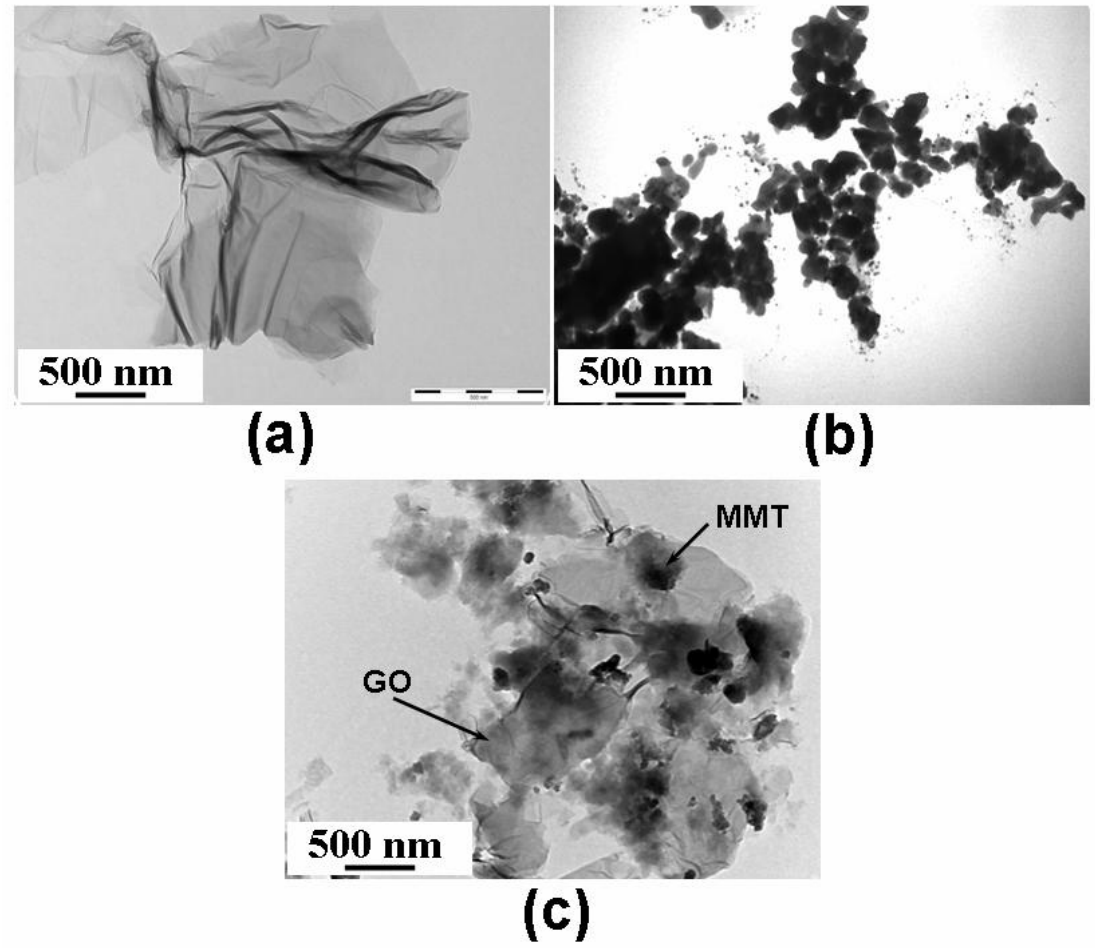

Fig. 5. TEM images of the GO (a), MMT (b) and GM (c).

The TEM clearly illustrated the flake-like shapes of GO (Fig. 5a), the size of GO was about 3~4 μm (length) × 2~3 μm (width). The partial folded structure of the GO might be due to the diversity of oxygen functionalities in thin GO layers. The TEM image of MMT (Fig. 5b) showed that the blocky structure of MMT picked up together, and the size of MMT was about 0.2~0.3 μm (length) × 0.2~0.3 μm (width). As shown in Fig. 5c, the

MMT nanoparticles were coated on the GO layers with a high density, and the wrinkled of GO was disappeared. Because of sonication, the appearance partially transparent and a little folded with isolated small fragments of GO on their surfaces, we also suggested that MMT was pillared in every layer of the GO. This conclusion was consistent with the SEM, EDX and XRD results. According to previous study,[38] exfoliated MMT nanoplatelets can partially reduce GO and both the hydrogen-bonding interactions and Na^+-mediated interactions between MMT and GO, then obtained the MMT-G hybrid films by vacuum filtration. In this work, ultra-sonication for 8h likely exfoliated the layered MMT, and the layered MMT was pillared in every layer of the GO to obtain the GM by drying.

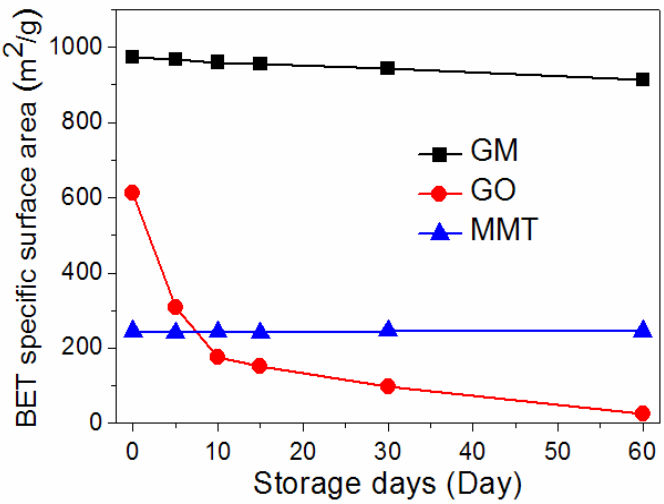

Fig. 6. The BET specific surface areas of GM, GO and MMT with different storage days in water.

As shown in Fig. 6, the BET specific surface area of GM, GO and MMT were 973, 612 and 245 $m^2 \cdot g^{-1}$, respectively. The discrepancy on as-obtained data and theoretical value of surface area of GO ($\geq$ 2000 $m^2 \cdot g^{-1}$) was attributed to the incomplete exfoliation and aggregation during reduction process because of the unavoidable van der Waals force between each single layer of GO. The higher BET specific surface area of GM than GO was due to the pillar of GO by MMT. With the increase of storage day, for example, after 60 days, the BET specific surface area of GO decreased to 26 $m^2 \cdot g^{-1}$, while the BET specific surface area of GM only decreased to 913 $m^2 \cdot g^{-1}$. π-π bonding interaction had been used to interpret the phenomenon. Since the GO contained π electrons to interact

with the π electrons of the nearby GO through the π-π electron coupling,[39] GO would reunite with the increase of storage day, while the reunite of GM was interrupted by MMT. These results showed that MMT could increase the storage stability.

3.2. Adsorption of dye and potentially toxic metal ion by GM, MMT or GO in single solution

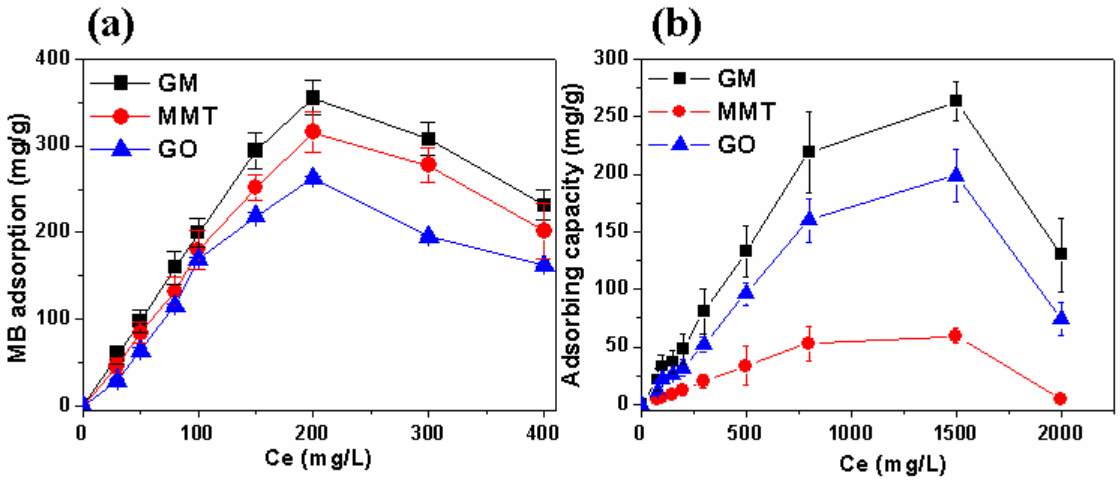

Fig. 7. Comparison of adsorptive capacities of MB (a) and Pb^{2+} (b) by different material (n=3).

We performed batch adsorption experiments of MB（C_0 = 0 to 400 mg/L）and Pb^{2+} (C_0 = 0 to 2000 mg/L) using GM, MMT and GO at 30 °C, pH = 5. As shown in Fig. 7, In the beginning, the adsorptions of MB and Pb^{2+} both increased with increasing concentration of MB and Pb^{2+}, while continuing to increase the concentration of MB and Pb^{2+} adsorption abilities down instead. Which might be explained that the concentration of MB and Pb^{2+} reached a certain degree, the adsorption had reached saturation and continued to increase the concentration of MB and Pb^{2+}, the adsorption sites would be competed which led to the decrease of the adsorption ability. According to the eq. (1), For removal of MB, the maximum adsorptions of GM, MMT and GO were 350, 315 and 265 mg/g, respectively (Fig. 7a), which indicated that the GM was able to adsorb more dye than alone MMT and alone GO; For removal of Pb^{2+}, the maximum adsorptions of GM, MMT and GO were 285, 136 and 60 mg/g, respectively (Fig. 7b), which indicated that the GM had the ability to adsorb more potentially toxic metal ion than alone MMT and alone GO.

The strong adsorptive ability of MMT for removing potentially toxic metal ion from aqueous solution had been reported in other literature.[40, 41] GO could be also served as an effective adsorbent towards dye.[39] In our study, we found that the adsorption property of GM was better than those of MMT and GO. Because the surface of GM in water was negatively charged (zeta potential = -30.4 mV), dissolved Pb^{2+} and MB that were positively charged would undergo attraction on approaching the anionic GM. On this basis, it was expected that Pb^{2+} and MB would have a strong sorption affinity for GM. In other word, the GM combined the properties of MMT and GO.

What is more, GM, MMT and GO expressed different adsorption speeds for MB and Pb^{2+}. The sorption of MB molecule was a noncovalent functionalization involving π-stacking interaction and corresponding to a weak binding energy, and the sorption of Pb^{2+} was an ionic bond interactions. The π-π bonding interaction and ionic bond interaction between adsorbent (GM, MMT or GO) and absorbable substances (MB or Pb^{2+}) was affected by the BET specific surface area. Since GM had larger BET specific surface area than MMT or GO, GM expressed faster adsorption speed than MMT or GO.

3.3. Adsorption study of dye- metal binary mixture

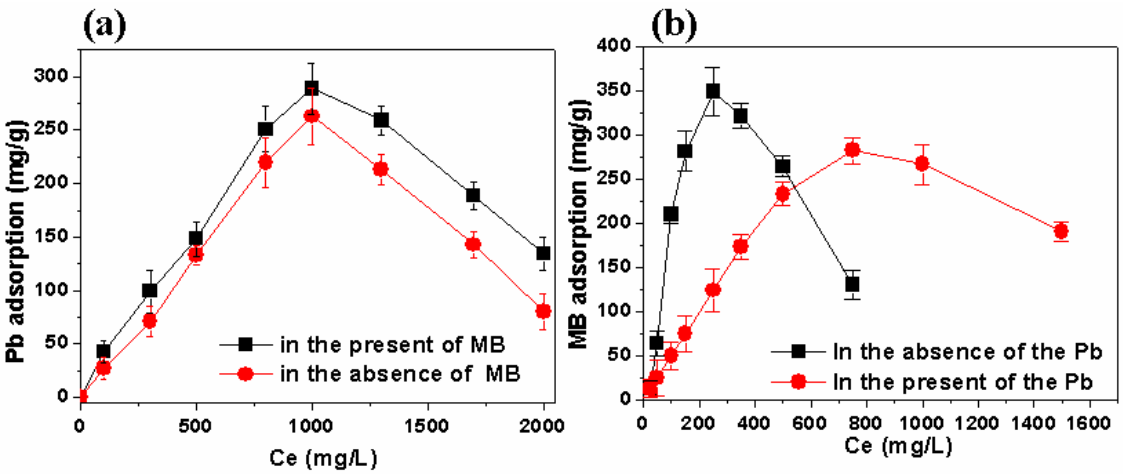

Fig. 8. (a) Effect of MB (C_0=150 mg/L) on the adsorption of Pb^{2+} by GM. (b) Effect of Pb^{2+} (C_0=150 mg/L) on the adsorption of MB by GM (n=3).

The adsorption of potentially toxic metal or dye by MMT and GO has been extensively studied and several review works have been reported in literature.[43] However,

most of these investigations only focused on the affinity of MMT and GO for single metal ion or dye. In this work, the simultaneous adsorption using dye-metal binary mixture had been considered, because the wastewater of some industries (e.g, automobile production and paper manufacturing) usually contained two types of pollutants. Firstly, we investigated the influence of MB (an initial concentration of 150 mg/L) on the adsorption of Pb^{2+} onto GM with different concentration of Pb^{2+} (0 to 2000 mg/L) at 30 °C, pH = 5. For GM, the adsorption capacity of Pb^{2+} in the presence of MB was slightly greater than that in the absence of MB (Fig. 8a), . It could be seen that about 31 mg/g of adsorbed Pb^{2+} was high in the presence of MB than that in the absence of MB according to the eq. (1). The results suggested MB would be favorable to be adsorbed on the GM surface and produce many organic functional groups in the GM surface, which caused the enhancement in the adsorption of Pb^{2+}. Then, the effect of Pb^{2+} (an initial concentration of 150 mg/L) on the adsorption of MB by GM with different concentration of MB (0 to 1500 mg/L) at 30 °C, pH = 5 was depicted in Fig. 8b. It could be seen that about 67 mg/g of adsorbed MB was less in the presence of Pb^{2+} than that in the absence of Pb^{2+} according to the eq. (1). This suggested that the active sites for metal ion and MB were similar, and the competitive adsorption between metal ion and MB made the adsorption of MB decrease.

3.4. Effects of pH and temperature on adsorption of GM

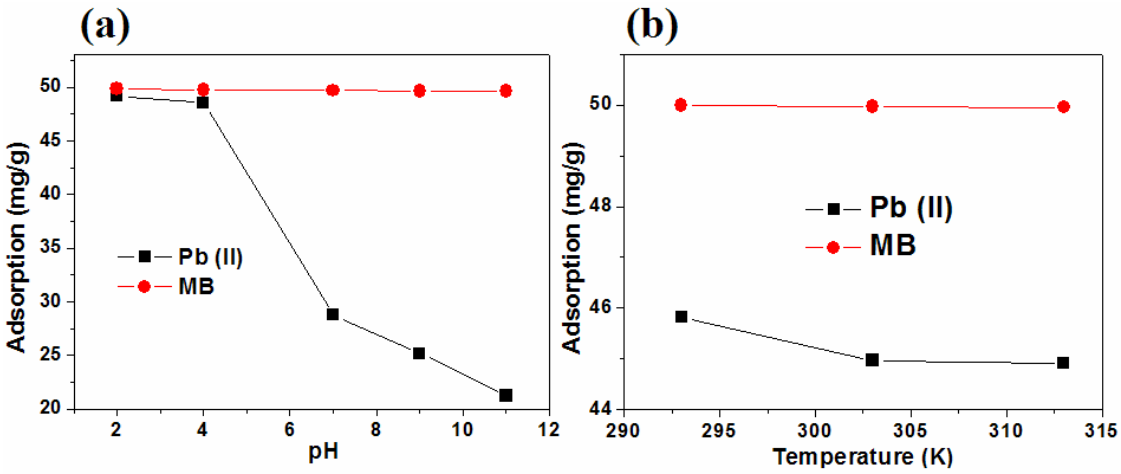

Fig. 9. (a) Effect of pH on MB-Pb^{2+} binary mixture by GM. (b) Effect of temperature on MB-Pb^{2+} binary mixture by GM.

It is well-known that the pH of the system was an important variable in the adsorption process. The variation of pH could affect the surface charge of the adsorbent, the degree of ionization and the speciation of the adsorbate. Fig. 9a showed the variation of adsorption of Pb^{2+} (200 mg/L) and MB (200 mg/L) on GM at various pH values. It was seen that higher pH value resulted in lower adsorption of Pb^{2+} while（the) adsorption of MB remained nearly unchanged with the increase of pH. The high uptake level of Pb^{2+} at low pH value could be attributed to the increased concentration of hydrogen (H^+) ion interacting with Pb^{2+}, leading to increased binding site on GM. As the pH was increased, removal of Pb^{2+} was inhibited possibly as a result of being flawed by precipitation as $Pb(OH)_2$ or a competition between hydroxyl ion and metal ion on the sorption site. For MB, adsorption kept nearly constant between 2 and 11. It might be because of the existence of Pb^{2+} prior to be effected by pH and the association of dye cation on solid would not take place easily, resulting in few increase in adsorption.

The effect of temperature on adsorptions of Pb^{2+} (200 mg/L) and MB (200 mg/L) was studied by changing the temperature from 20 to 40 °C, and the results were presented in Fig. 9b. The adsorption capacities of Pb^{2+} was decreased and MB was slightly decreased at temperature ranged from 20 to 40 °C, which indicated that the adsorption process of MB-Pb^{2+} binary system on the GM adsorbent was an exothermic process. So, the optimum temperature for adsorptions of Pb^{2+} and MB was elected to be 20 °C. Standard free energy change (ΔG^0) provided information about the interaction between the surface of GM and the MB or Pb^{2+}. The ΔG^0 could be calculated from the relationship.[44]

$$\Delta G^0 = RT \ln K_C \qquad (2)$$

$$K_C = \frac{q_e}{C_e} \qquad (3)$$

where C_e (mg/L) and q_e (mg/g) were the concentration and adsorption capacity at the equilibrium, respectively. Kc was the thermodynamic equilibrium constant, R was the universal gas constant 8.314 J $mol^{-1}K^{-1}$ and T was the absolute temperature. ΔG^0 calculated from eqs. (2) and (3) were listed in Table 1.

Table 1

ΔG^0 values of adsorptions of MB and Pb^{2+} on GM at 20, 30, 40 °C.

	20 °C (293.15K)	30 °C (303.15K)	40 °C (313.15K)
ΔG^0 (MB)	-4.146	-3.775	-3.864
ΔG^0 (Pb^{2+})	-18.747	-16.650	-16.453

The negative ΔG^0 values at different temperature indicated the spontaneous nature of the adsorptions of Pb^{2+} and MB onto the adsorbent of GM. The more negative value with the decrease of temperature showed that the amount adsorbed at equilibrium must increase with the decreasing temperature.

3.5. Effect of contact time on adsorption of GM

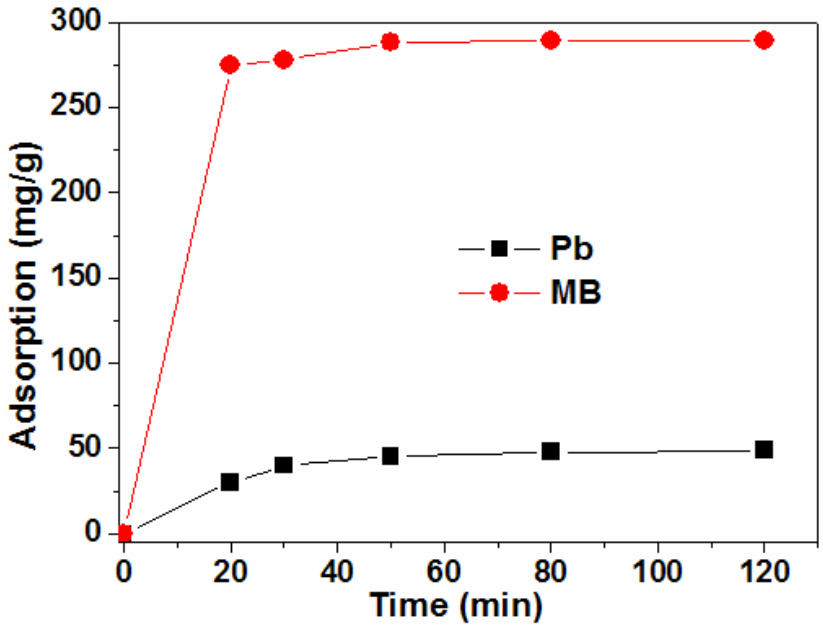

Fig. 10. Effect of contact time on MB and Pb^{2+} by GM.

Fig. 10 presented the dynamic adsorption of MB (200 mg/L) and Pb^{2+} (200 mg/L) on the GM at 30 °C, pH = 5. During the adsorption process, It was seen that MB adsorption was gradually increased and reached an equilibrium adsorption of 298 mg/g at 50 min; Pb^{2+} adsorption was also increasing with the time but the equilibrium adsorption was slightly reduced, the equilibrium adsorption was 49 mg/g. Therefore, GM was

suitable for efficient removal of potentially toxic metal ion and dye.

3.6. Adsorption mechanism

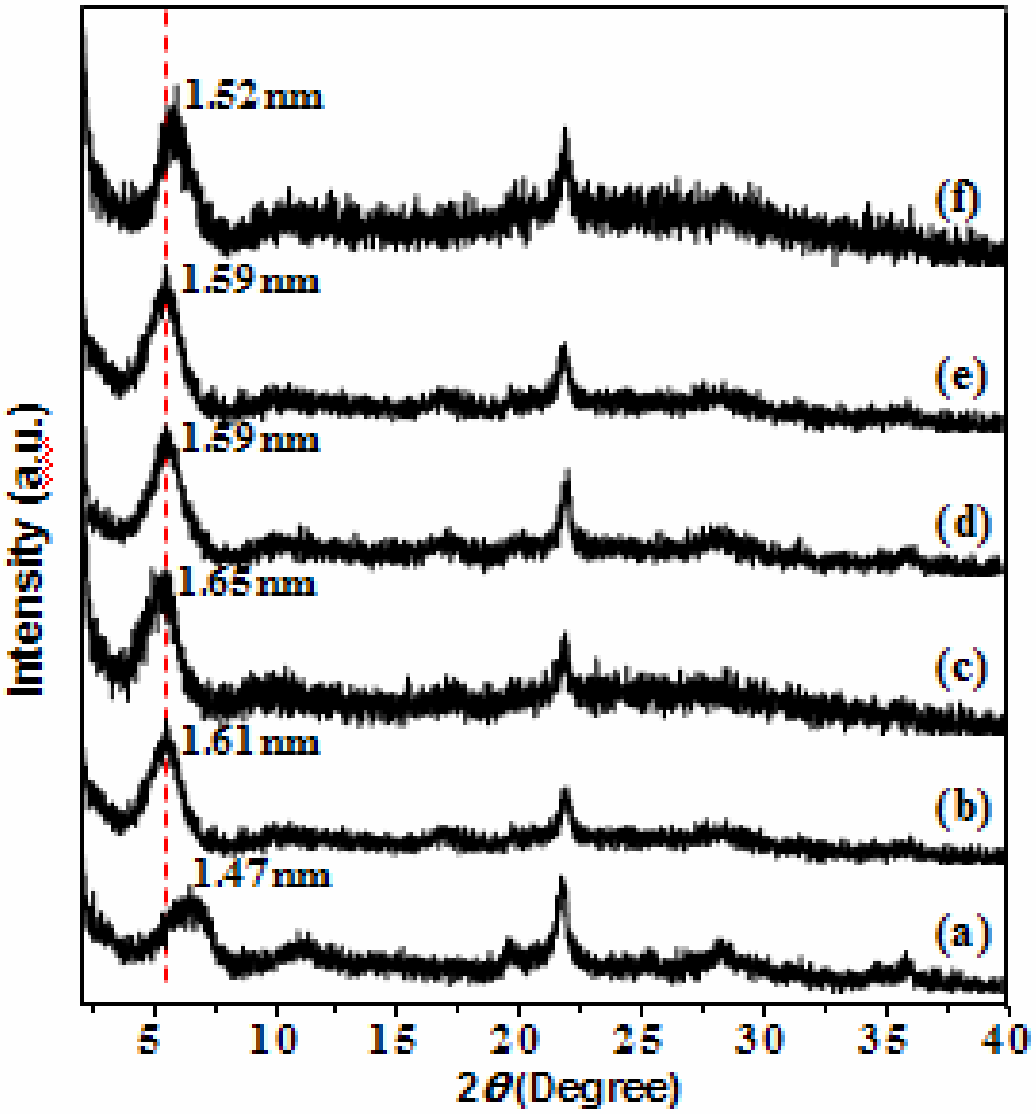

Fig. 11. XRD patterns: (a) GM, (b) GM adsorbed MB, (c) GM adsorbed MB and then adsorbed Pb^{2+}, (d) GM adsorbed Pb^{2+}, (e) GM adsorbed Pb^{2+} and then adsorbed MB, and (f) GM adsorbed MB and Pb^{2+} simultaneously.

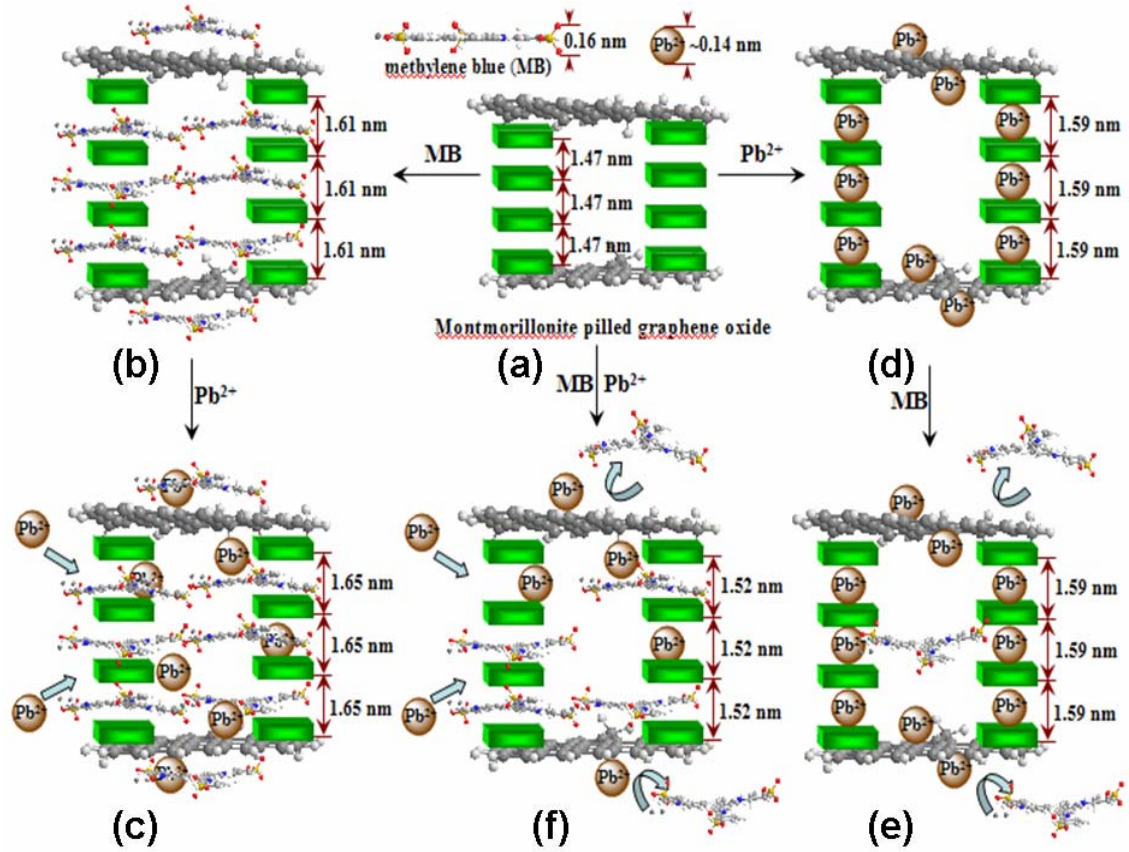

Fig. 12. Adsorption mechanism: (a) GM, (b) GM adsorbed MB, (c) GM adsorbed MB and then adsorbed Pb^{2+}, (d) GM adsorbed Pb^{2+}, (e) GM adsorbed Pb^{2+} and then adsorbed MB and (f) GM adsorbed MB-Pb^{2+} simultaneously.

In order to illustrate the mechanism of synergistic and competitive adsorption of potentially toxic metal ion and dye on GM, XRD study was performed (Fig. 11), and the corresponding adsorption mechanism was showed in Fig. 12. As shown in Fig. 11a, a typical diffraction peak of GM at 6.07° was corresponded to a basal spacing of 1.47 nm (Fig. 12a). When MB was adsorbed on GM, the peak was moved to a low angle at 5.46°, which was corresponded to a basal spacing of 1.61 nm (Fig. 11b and Fig. 12b). then, Pb^{2+} was adsorbed on GM, the peak was moved to a low angle at 5.35°, which was corresponded to a basal spacing of 1.65 nm (Fig. 11c and Fig. 12c); When Pb^{2+} was adsorbed on GM, the peak was moved to a low angle at 5.54°, which was corresponded to a basal spacing of 1.59 nm (Fig. 11 and Fig. 12d). then, MB was adsorbed on GM, the peak was unchanged, which was corresponded to a basal spacing of 1.59 nm (Fig. 11e

and Fig. 12e); When Pb^{2+} and MB were adsorbed on GM at the same time, the peak was moved to a low angle at 5.79°, which was corresponded to a basal spacing of 1.52 nm (Fig. 11f and Fig. 12f).

In previous study, a multi-component solution might exhibit three possible types of adsorption effects under competitive condition: a) synergism: the effect of the mixture was greater than that of the individual sorbate in the mixture; b) antagonism: the effect of the mixture was less than that of the individual sorbate in the mixture; c) non-interaction: the mixture had no effect on the adsorption of each sorbate in the mixture.[44]

In our study, first of all, compared with that of GM (Fig. 12a), the basal spacing of MB-adsorbed GM (Fig. 12b) and Pb^{2+}-adsorbed GM (Fig. 12c) were increased 0.14 and 0.12 nm, respectively. As shown in Fig. 12a, the diameters of MB and Pb^{2+} were 0.16 and 0.14 nm, respectively, which suggested that the MB and Pb^{2+} could adsorb into the layer of GM; secondly, compared with MB-adsorbed GM (Fig. 12b), the basal spacing of MB-adsorbed, then Pb^{2+}-adsorbed GM (Fig. 12c) was increased, which indicated that the MB-adsorbed GM had synergistic adsorption effect to Pb^{2+} adsorption onto the GM. Compared with Pb^{2+}-adsorbed GM (Fig. 12d), the basal spacing of Pb^{2+}-adsorbed, then MB-adsorbed GM (Fig. 12e) was unchanged, which indicated that the Pb^{2+}-adsorbed GM had antagonistic adsorption effect to MB adsorption onto the GM. As for GM adsorb MB-Pb^{2+} binary mixture (Fig. 12f), the basal spacing was decreased than the basal spacing of MB-adsorbed GM (Fig. 12b) or Pb^{2+}-adsorbed GM (Fig. 12c), which indicated that the GM adsorbed MB-Pb^{2+} binary mixture had antagonistic adsorption effect to each other onto the GM. These results were in accordance with those of Fig. 8; thirdly, the effect of Pb^{2+} on MB adsorption could mainly be explained by the reaction occurring at the surface of the GM (Fig. 12e). The adsorption of Pb^{2+} on the surface of GM might affect MB adsorption throughout the following mechanisms: (1) Pb^{2+} was bound to the same sites on GM surface as MB; (2) Pb^{2+} was attached to GM surface through a mechanism different from MB, and the total sites available for subsequent MB adsorption remained the same, but a layer of Pb^{2+} adsorbed on the surface of GM might produce a barrier for MB to connect to the available adsorption sites.[45] On the contrary, the effect of MB on Pb^{2+} adsorption might account for the adsorption of MB on GM (Fig. 12c), causing an increase in the surface negative charges, which might favor the adsorption of

Pb^{2+}. In addition, MB was adsorbed on the GM surface and produced more organic functional groups in the GM-MB surface, which caused an enhancement in the Pb^{2+} adsorption.

4. Conclusion

In this study, MMT-pillared GO as an adsorbent was prepared. Due to the pillar of GO by MMT, the BET specific surface area of GM (973 $m^2 \cdot g^{-1}$) was higher than that of GO (612 $m^2 \cdot g^{-1}$). The GO reunited with the increase of storage day, while the reunite of GM was interrupted by MMT. The GM expressed faster adsorption speeds than GO. In single systems, GM showed much higher adsorption of MB and Pb^{2+} than MMT or GO. In binary-adsorbate system, higher solution pH resulted in lower adsorption in Pb^{2+} while MB adsorption remained unchanged with the increasing pH. The adsorption capacity of Pb^{2+} and MB both decreased when the temperature ranged from 20 to 40 °C, which indicated that the adsorption process of MB-Pb^{2+} binary system on the GM adsorbent was an exothermic process. The adsorption mechanism shown that the presence of MB enhanced the adsorption efficiency of Pb^{2+} on GM, while the existence of Pb^{2+} decreased the adsorption capacity of MB on GM. As GM was easily obtained and cheap, it would be promising for removal of potentially toxic metal ions and dyes.

Acknowledgments

The authors acknowledge financial support from the National Natural Science Foundation of China (51172099, 21006038 and 21376104), the Foundation of Science and Technology Projects of Guangdong Province (2011B090300018), the Fundamental Research Funds for the Central Universities (21612109), the Research and innovation project of Jinan University for Excellent Master (201321), and the 2013 Jinan University Challenge Cup for Student Extracurricular Academic Science and Technology Work Competition (201312B07 and 201312B49). Dongliang Wan and Jinglin Zhang contributed equally to this work.

References

[1] B. Prelot, V. Einhorm, F. Marchandeau, J. M. Douillard, J. Zajac, J. Colloid Interface

Sci. 2012. **386**. 300.

[2] L. Campbell, D. G. Dixon, R. E. Hecky, J. Hazard. Mater. 2006. **136**. 482.

[4] L. Mouni, D. Merabet, A. Bouzaza, L. Belkhiri, Desalination. 2011. **276**. 148.

[5] R.A. Goyer, Environ. Health Perspect. 1993. **100**. 177.

[6] T. Wu, X. Cai, S. Z. Tan, H. Y. Li, J. S. Liu, W. D. Yang, Chem. Eng. J. 2011. **173**. 144.

[7] C. A. P. Almeida, N. A. Debacher, A. J. Downs, L. Cottet, C. A. D. Mello. J. Colloid Interface Sci. 2009. **332**. 46.

[8] S. T. Yang, S. Chen, Y. L. Chang, A. Cao, Y. F. Liu, H. F. Wang. J. Colloid Interface Sci. 2011. **359**. 24.

[9] S. K. Porter, K. G. Scheckel, C. A. Impellitteri, A. Ryan, Rev. Environ. Sci. Technol. 2004.**34**. 495.

[10] J. L. Gardea-Torresdey, G. de la Rosa, J. R. Peralta-Videa, Pure Appl. Chem. 2004. **76**. 801.

[11] M. Pansini, Miner. Deposita. 1996. **31**. 563.

[12] S. B Wang, T. Terdkiatburana, M.O. Tadé, Sep. Purif. Technol. 2008. **58**. 353.

[13] E. Repo, J. K. Warchoł, A. Bhatnagar, M. Sillanpää, J. Colloid Interface Sci. 2011. **358**. 1261.

[14] S. J. Allen, G. McKay, J. F. Porter, J. Colloid Interface Sci. 2004. **280**. 322.

[15] M. Y. Chang, R. S. Juang, J. Colloid Interface Sci. 2004. **278**. 18.

[16] A. Bhatnagar, A. K. Jain, J. Colloid Interface Sci. 2005. **281**. 49.

[17] V. K. Gupta, A. Mittal, V. Gajbe, J. Colloid Interface Sci. 2005. **284**. 89.

[18] M. Choi, J. Jang, J. Colloid Interface Sci. 2008. **325**. 287.

[19] L. D. Pablo, M. L. Chávez, M. Abatal, Chem. Eng. J. 2011. **171**. 1276.

[20] J. Zhu, V. Cozzolino, M. Pigna, Q. Y. Huang, A. G. Caporale, A. Violante, Chemosphere. 2011. **84**. 484.

[21] S. B. Wang, H. Q. Sun, H. M. Ang, M. O. Tadé, Chem. Eng. J. 2013. **226**. 336.

[22] D. Ma, J. T. Lin, Y. Y. Chen, W. Xue, L. M. Zhang, Carbon. 2012. **50**. 3001.

[23] S. H. Abhishek, W. I. Choi, G. Tae, Chem. Commun. 2012. **48**. 5820.

[24] Z. Y. Sui, Y. Cui, J. H. Zhu, B. H. Han, Appl. Mater. Interfaces. 2013. **5**. 9172.

[25] O. S. Chan, W. H. Cheng, G. McKay, Chem. Eng. J. 2012. **191**. 162.

[26] M. S. Chiou, G. S. Chuang, Chemosphere. 2006. **62**. 731.

[27] G. Atun, E. T. Acar, Sep. Sci. Technol. 2010. **45**. 1471.

[28] D. L. Zhao, G. D. Sheng, C. G. Chen, X. K. Wang, Appl. Catalysis B: Environ, 2012, 111, 303

[29] G. Zhao, S. Song, C. Wang, et al., Adv. Mater. 2011, **23**, 3959.

[30] D. Mohan, K. P. Singh, Water Res. 2002. **36**. 2304.

[31] G. X. Yang, H. Jiang. Environ. Sci. Technol. 2011, **45**, 10454.

[32] X. Cai, S. Z. Tan, A. G. Xie, M. S. Lin, Y. L. Liu, X. J. Zhang, Z. D. Lin, T. Wu, W. J. Mai, Mater. Res. Bull. 2011. **46**. 2353.

[33] X. Cai, S. Z. Tan, M. S. Lin, A. G. Xie, W. J. Mai, X. J. Zhang, Z. D. Lin, T. Wu, Y. L. Liu, Langmuir. 2011. **27**. 7828.

[34] X. Cai, S. Z. Tan, A. L. Yu, J. L. Zhang, J. H. Liu, W. J. Mai, Z. Y. Jiang, Chem. – Asian J. 2012. **7**. 1664.

[35] C. M. Chen, Q. H. Yang, Y. G. Yang, Y. F. Wen, P. X. Hou, M. Z. Wang, H. M. Cheng, Adv. Mater. 2009. **21**. 3007.

[36] X. Cai, M. S. Lin, S. Z. Tan, W. J. Mai, Y. M. Zhang, Z. W. Liang, Z. D. Lin, X. J. Zhang, Carbon. 2012. **50**. 3407.

[37] H. H. Murray, Oxford, 2007.

[38] C. Zhang, W. W. Tjiu, W. Fan, Z. Yang, S. Huang, T. Liu, J. Mater. Chem. 2011. **21**. 18011.

[39] Z. G. Pei, L. J. Li, L. X. Sun, S. Z. Zhang, X. Q. Shan, S. Yang, B. Wen, Carbon. 2013. **51**. 156.

[40] S. H. Lin, R. S. Juang, J. Hazard. Mater. 2002. **92**. 315.

[41] L. D. Pabloa, M. L. Chávezb, M. Abatala, Chem. Eng. J. 2011. **171**. 1276.

[42] G. K. Ramesha, A. Vijaya Kumara, H. B. Muralidhara, S. Sampath, J. Colloid Interface Sci. 2011. **361**. 270.

[43] V. K. Upadhyayula, S. G. Deng, M. C. Mitchell, G. B. Smith, Sci. Total Environ. 2009. **408**. 1-13.

[44] V. Hernández-Montoya, M. A. Pérez-Cruz, D. I. Mendoza-Castillo, M. R. Moreno-Virgen, A. Bonilla-Petriciolet, J. Environ. Manage. 2013. **116**. 213.

[45] T. Terdkiatburana, S. B. Wang, M. O. Tadé, Chem. Eng. J. 2008. **139**. 437.